Mechanical switching of ferro-electric rubber

J. M. Adams and M. Warner[1]

[1] *Cavendish Laboratory, University of Cambridge, Madingley Road, Cambridge CB3 0HE, U.K.*

(Dated: March 4, 2007)

At the A to C transition, elastomers have been recently observed to undergo ∼35% spontaneous shear strains. We describe how strains of up to twice this value can be mechanically induced in SmC elastomers. For typical sample geometries, microstructures akin to those seen in nematic elastomers should arise. We give explicit results for the nature of the textures. Chiral SmC elastomers are ferro-electric. We describe how the polarisation can be mechanically reversed by large, hard or soft strains of the rubber, depending upon sample geometry.

PACS numbers: 61.30.Vx , 83.80.Va, 62.20.Dc and 61.41.+e

I. INTRODUCTION

One of the most remarkable properties of liquid crystals is their ferro-electricity when in the chiral smectic C (SmC*) phase [1]. Unlike crystalline ferro-electrics, their polarisation is easily switched, for they are liquids, albeit with orientational (nematic) and layered (smectic) order. Thus new types of displays have been based on the fast and ready response of such liquids to electric fields [2, 3]. We model the mechanically-driven switching of soft-solid analogues – SmC* elastomers with both orientation and layering where imposed strains can rotate the polarisation, $\mathbf{P}$.

Nematic order, about an ordering director $\hat{\mathbf{n}}$, is along the layer normal $\hat{\mathbf{k}}$, in smectic A (SmA) phases. RB Meyer *et al* [1] recognised that when $\hat{\mathbf{n}}$ tilts with respect to $\hat{\mathbf{k}}$ on entering the SmC phase, then in a chiral system polarisation can exist: denote the direction of the projection of $\hat{\mathbf{n}}$ in-plane by the unit vector $\hat{\mathbf{c}}$, whence $\hat{\mathbf{k}}\wedge\hat{\mathbf{c}}\rightarrow\hat{\mathbf{p}}$ is an operation that defines a polar unit vector $\hat{\mathbf{p}}$ in a chiral system. Fig 1 shows the A and C phases, with smectically ordered rods rather more sharply confined to layers than is realistic.

Liquid crystalline (LC) polymers display the same phases as classical materials. The rods, in the sketch fig 1, are pendant to main chains which can then be linked to form an LC elastomer. Nematic elastomers suffer large mechanical elongations/contractions on cooling/heating to and from the ordered state. If strains are applied non-coaxially with $\hat{\mathbf{n}}$, director rotation and further sympathetic shears can develop to allow shape change without energy cost in ideal systems, and with little energy cost in non-ideal systems — so-called soft elasticity [5, 6]. The magnitude of spontaneous distortion on entering the nematic state sets the scale for the extent of soft deformation when mechanically-induced director rotation occurs.

SmA elastomers are not soft because (a) the director is not free to rotate without taking the layers with it and (b) the matrix can only deform while affinely convecting its embedded layers with it and respecting the constancy of layer spacing. The smectic layer modulus is much larger than the rubber modulus and hence distortions such as extension along $\hat{\mathbf{k}}$ are very expensive and in most systems only occur to small amplitude [7, 8] before instabilities arise. Essentially SmA rubbers behave 2-dimensionally; they stretch and contract in-plane only. Their shears have either displacements purely in-plane or, if out of plane, they act to rotate the layers. SmA rubber elasticity is highly complex and non-linear.

The same constraints of constancy of layer spacing act on SmC elastomers. The transition SmA→SmC is accompanied by a spontaneous shear, Λ, not trivially related to the molecular tilt angle θ [4, 9–11]. This shear has been shown to be large, $\Lambda\sim 0.3-0.4$ in the experiments of [4], Fig. 1(c) and (d). We take subsequent distortions with respect to the spontaneously distorted shape of Fig. 1(b) or (d), that is the reference state shown relaxed and without distortion in Fig. 2(a). (A residual shear visible in the SmA state, Fig. 1(c), is an artefact of the 2-step cross-linking method of achieving monodo-

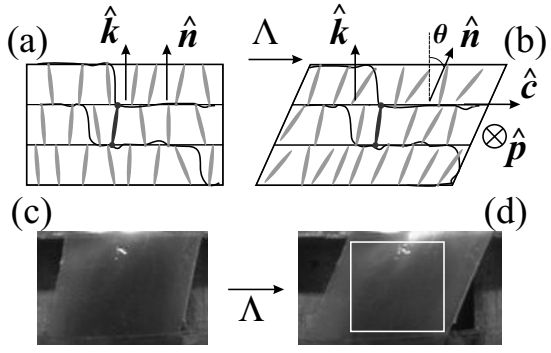

FIG. 1: (a) Smectic A phase with parallel director $\hat{\mathbf{n}}$ and layer normal $\hat{\mathbf{k}}$. The polymer backbones are for the polymeric case with the rods shown a pendant. A crosslink (dots at either end of the rod) links polymers into the network. (b) Smectic C phase with $\hat{\mathbf{n}}$ tilted by θin a direction defined by the unit vector $\hat{\mathbf{c}}$ in the plane. The third (unit) direction, $\hat{\mathbf{p}}=\hat{\mathbf{k}}\wedge\hat{\mathbf{c}}$, is into the page. It defines the direction of polarization, $\mathbf{P}=P\hat{\mathbf{p}}$. For SmC elastomers, there is a spontaneous shear Λ with respect to its SmA parent. (c) and (d) Photographs [4] of the A to C transition in elastomers. The cut out in (d) represents the sample in Fig. 2(a) that is to be deformed.

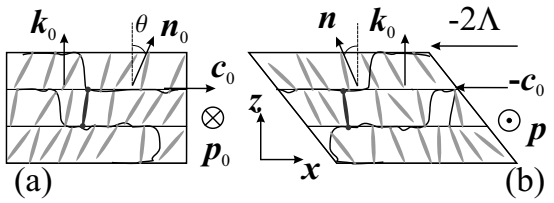

FIG. 2: A block of SmC rubber (a) initially undistorted with $\hat{\mathbf{n}}_0$ and $\hat{\mathbf{c}}_0 \equiv \hat{\mathbf{x}}$. The layer normal will be taken to remain along $\hat{\mathbf{z}}$. (b) sheared by $\lambda_{xz} = -2\Lambda$ with respect to its relaxed state. The in-plane director has reversed, $\hat{\mathbf{c}} \to -\hat{\mathbf{c}}_0$ and thus also the polarisation direction: $\hat{\mathbf{p}}_0 \to \hat{\mathbf{p}} = -\hat{\mathbf{p}}_0$.

mains.)

SmC elastomers can theoretically be soft since the vector $\hat{\mathbf{c}}$ can rotate about $\hat{\mathbf{k}}$ and in doing so induces shape changes of the body without change of the smectic or rubber elastic energy. Soft elasticity has been recovered and in general is predicted to be of considerable complexity in SmC elastomers since the layer normal can also rotate [9, 12]. One can find [12] concrete examples of soft modes where the layer normal remains fixed. We denote the angle of rotation of $\hat{\mathbf{c}}$ about $\hat{\mathbf{k}}_0$ by ϕ. The soft shape changes associated with changing ϕ are shears which conclude at $\phi = \pm\pi$, with $\lambda_{xz} = -2\Lambda$ and all other distortions vanishing. In Fig. 2(b) this final shear corresponds to reversing the spontaneously sheared shape in Fig. 1(b) to its opposite form. The spontaneous simple shear thus has an important role in delineating the extent of softness of imposed deformations in smectic rubbers. Analogously, in experiment and theory of softness in nematic elastomers, the extent is delineated by the extent of spontaneous elongation on entering the nematic phase. For ϕ increasing still further, the original undistorted state is eventually regained at $\phi = 2\pi$.

As $\hat{\mathbf{c}}$ rotates about $\hat{\mathbf{k}}$ by ϕ, then so too does the polarisation direction $\hat{\mathbf{p}}$. If it is initially along $\hat{\mathbf{y}}$, then when $\hat{\mathbf{c}}$ has rotated by π, $\hat{\mathbf{p}}$ has reversed to $-\hat{\mathbf{y}}$, see Fig. 2(b). The remainder of this paper is concerned with describing how this reversal of polarisation can be achieved by the imposition of shear deformation to the elastomer. The applications of shear generating large electrical changes are obvious and very attractive.

Although it is possible to find soft trajectories of deformation that reverse $\hat{\mathbf{p}}$, these will not in general satisfy boundary conditions imposed by, say, rigid electrodes or clamps. One can, in some cases, take combinations of $\pm\phi$ deformations that form a texture that overall satisfies the external constraints, that is the free energy has been "quasi-convexified" [13], a process well-understood in the routes to soft deformation of nematic elastomers [6, 14]. We show such a solution for SmC elastomers. The general mathematical problem of how textures in SmC elastomers make possible soft deformations in the presence of constraints has been attacked by Adams *et al* [15]. Otherwise, SmC elastomers can deform via non-soft alternatives [15] that fully satisfy constraints, but these will also require textures that we also calculate here. In either case there will be barriers (possibly smaller for soft textures) between the two states of reversed polarisation. The choice between soft and non-soft alternatives will depend upon whether one has sheet or slab geometry — we discuss both choices in Section III. In any event, we hope that the range of deformation paths we describe will urgently stimulate experiment to explore the ferro-electric response of smectic elastomers to shears opposed to the spontaneous distortion that arises on leaving the A-state. Our theoretical models will show how completely open the understanding of these systems is.

II. A MODEL FOR NON-LINEAR DISTORTIONS OF SMECTIC-C RUBBER

We adopt a particular model model that successfully describes the non-linear rubbery and smectic elasticity of SmA elastomers, and which has also been applied to SmC elastomers. The underlying nematic rubbery elasticity is subject only to layers moving affinely with the bulk and only allowing distortions that then respect the constancy of layer spacing. Thus material points $\mathbf{R}_0$ and layer normals $\hat{\mathbf{k}}_0$ in the reference state transform as [8]:

$$\mathbf{R} = \underline{\underline{\lambda}} \cdot \mathbf{R}_0 \quad \text{and} \quad \hat{\mathbf{k}} = \underline{\underline{\lambda}}^{-T} \cdot \hat{\mathbf{k}}_0 \tag{1}$$

with $\underline{\underline{\lambda}}$ the deformation gradient. It is evidently rigidly constrained so that $|\underline{\underline{\lambda}}^{-T} \cdot \hat{\mathbf{k}}_0| = 1$ where $-T$ denotes transposed inverse. $\text{Det}\left(\underline{\underline{\lambda}}\right) = 1$ expresses constancy of volume, required in all elastomers since their shape-changing deformations are at much lower energy than the cost of volume change. The free energy density and a general soft deformation are respectively:

$$f = \tfrac{1}{2}\mu \text{Tr}\left(\underline{\underline{\ell}}_0 \cdot \underline{\underline{\lambda}}^T \cdot \underline{\underline{\ell}}_n^{-1} \cdot \underline{\underline{\lambda}}\right) \quad \text{and} \quad \underline{\underline{\lambda}}_s = \underline{\underline{\ell}}_n^{1/2} \cdot \underline{\underline{W}} \cdot \underline{\underline{\ell}}_0^{-1/2} \tag{2}$$

with $\underline{\underline{W}}$ a general rotation matrix in the nematic case [16], and a more specialised form for smectic elastomers [12]. The shear modulus of the isotropic state of the elastomer is $\mu \sim 10^5 - 10^6 \text{J/m}^3$, nearly two orders of magnitude smaller than the smectic layer spacing modulus for elastomers and 4 orders of magnitude smaller than the bulk modulus – thus the rigid constraints on $\underline{\underline{\lambda}}$ discussed above. We discuss in Appendix A how μ can be estimated by measurements in the Sm state. The shape tensors of the network polymers, $\underline{\underline{\ell}}_0$ initially and $\underline{\underline{\ell}}_n$ after deformation (when the director $\hat{\mathbf{n}}_0$ has possibly rotated to the new direction $\hat{\mathbf{n}}$) are of the form $\underline{\underline{\ell}}_0 = (r-1)\hat{\mathbf{n}}_0\hat{\mathbf{n}}_0 + \underline{\underline{\delta}}$ where r is the anisotropy in the distribution of polymer shapes. These tensors encode information about the direction of order. We take the distribution for simplicity to be uniaxial. This approximation is discussed in [12] —

effects due to rotation of the long axis of the anisotropic distribution are very large and give a first order description of a system that in reality is certainly to an extent biaxial. The minimum free energy is $3\mu/2$ which obtains when there is no distortion, $\underline{\underline{\lambda}} = \underline{\underline{\delta}}$ and no director rotation, $\hat{\mathbf{n}} = \hat{\mathbf{n}}_0$ and hence $\underline{\underline{\ell}}_n^{-1} = \underline{\underline{\ell}}_0^{-1}$, or when deformations are soft, $\underline{\underline{\lambda}}^s = \underline{\underline{\lambda}}$.

The spontaneous shear $\lambda^{\rm c}_{xz}$ in this model, denoted here by Λ, is given by

$$\lambda^{\rm c}_{xz} \equiv \Lambda = (r-1)\sin\theta\cos\theta/\rho \qquad (3)$$

where the combination $\rho = r\cos^2\theta + \sin^2\theta \leq r$ will repeatedly follow in the concrete examples of distortions we shall give. The molecular details are thus simply encoded. At fixed temperature, θ does not change if we also assume that anchoring is rigid, that is applied strains do not mechanically alter the tilt angle. In considering elastomers with extreme anisotropy of mechanical properties, we are implicitly dealing with smectic elastomers where the layer structure and other details of molecular ordering are on a higher energy scale than rubber elasticity [7]. There may be systems in which tilt is not rigid under imposed strains, a possibility that has been considered theoretically [9, 11]. It is possible that the chain anisotropy r might change with tilt θ and thus that the θ dependence is more complicated than appears in eqn (3). This complication will not concern us for elastomers at fixed temperature, and thus fixed tilt, during mechanical experiments. We are not dealing with smectic elastomers in which layers do not appear to significantly effect mechanical properties, for instance elastomers where one can induce compression of the smectic layers by applying an in-plane strain [17].

A. Simple, non-soft response to shear

We are interested in shearing SmC elastomers simply, without rotating or distorting the layers, perhaps by fixing rigid plates to their xy surfaces. Firstly, consider a simple, non-soft deformation with its inverse transpose:

$$\underline{\underline{\lambda}} = \begin{pmatrix} 1 & 0 & \lambda_{xz} \\ 0 & 1 & \lambda_{yz} \\ 0 & 0 & 1 \end{pmatrix}; \quad \underline{\underline{\lambda}}^{-T} = \begin{pmatrix} 1 & 0 & 0 \\ 0 & 1 & 0 \\ -\lambda_{xz} & -\lambda_{yz} & 1 \end{pmatrix}. \qquad (4)$$

Trivially $\mathrm{Det}\left(\underline{\underline{\lambda}}\right) = 1$, volume is conserved, and $\underline{\underline{\lambda}}^{-T}\cdot\hat{\mathbf{z}} = \hat{\mathbf{z}}$, the layer normals are not rotated and their separation is unchanged by the action of $\underline{\underline{\lambda}}$. The 0 and 1 entries in (4) ensure that the xy plates do not change shape.

We take an initial $\hat{\mathbf{c}}_0 = \hat{\mathbf{x}}$ as in Fig. 2(b) and impose a shear λ_{xz}. The shear λ_{yz} is the relaxation expected as $\hat{\mathbf{n}}$ is induced to rotate by ϕ about $\hat{\mathbf{k}}$ towards $\hat{\mathbf{y}}$. Inserting $\underline{\underline{\lambda}}$ into f, and minimizing over λ_{yz} and ϕ gives the optimal free energy and relaxation as a function of λ_{xz}. Because

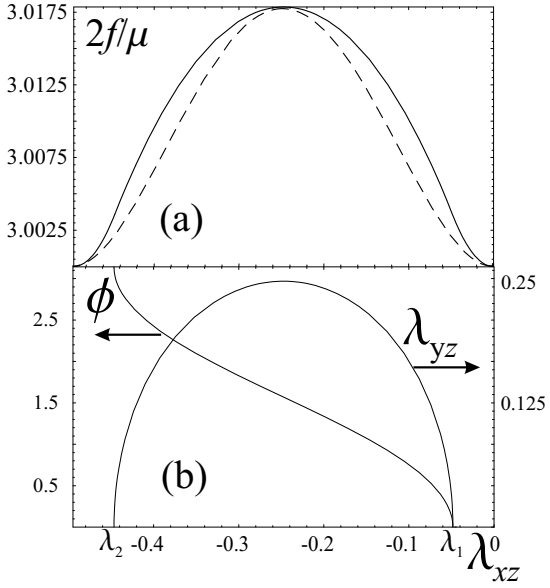

FIG. 3: (a) The elastic free energy, in units of $\frac{1}{2}\mu$, against imposed shear $\lambda_{xz} \leq 0$. The dotted line is energy allowing yx relaxation. (b) Rotation ϕ of the in-plane director $\hat{\mathbf{c}}$ about the layer normal, and the concomitant yz shear relaxation, both starting and concluding at thresholds λ_1 and λ_2 respectively. The anisotropy is $r = 2$ and the director tilt is $\theta = \pi/6$.

the $\underline{\underline{\lambda}}$ of eqn (4) is not soft (there is a cost of constraining diagonal elements to 1 and some shears to 0), in fact there is a threshold, λ_1, before λ_{yz} relaxation and rotation of $\hat{\mathbf{c}}$ starts. Until then the free energy is hard with a corresponding modulus, see the curvature of the initial part of Fig. 3(a), and full details in Appendix A. For the $r = 2$, $\theta = \pi/6$ chosen for illustration throughout, the spontaneous shear would be $\Lambda = \sqrt{3}/7 \simeq 0.246$. When relaxation starts, the free energy is softened considerably since now shape change can be more by rotation of the long axis of the polymer chain distribution than by an expensive distortion of the chains. The shear λ_{yz} and rotational ϕ relaxation, Fig. 3(b), are both initially singular. Director rotation is directly observable optically. We defer discussing it until we consider sample geometry and the questions of textures and ferro-electric switching. The thresholds are slightly complicated functions of r and θ that can be found analytically from the free energy.

The yz shear reaches a maximum numerically equal to Λ at $\phi = \pi/2$ and $\lambda_{xz} = -\Lambda$ since at this imposed shear $\hat{\mathbf{c}}$ points along $\hat{\mathbf{y}}$. The anisotropy now along $\hat{\mathbf{y}}$ is completely analogous to the tilt of the anisotropy along $\hat{\mathbf{x}}$ in Fig. 1(b) with the same yz-shear developing as was the case with xz-shear in going from SmA to SmC in Fig. 1. The free energy is maximal at this shear and then declines back to its minimal value $3\mu/2$ when the imposed shear is -2Λ. The yz-relaxation vanishes, and ϕ attains π, in a singular manner at a threshold, λ_2, equivalent

to that at small λ_{xz}, before the xz shear reaches -2Λ. In non-ideal systems (semi-soft elastomers) the free energy would not be at an absolute minimum at $\phi = \pi$. The singular behaviour is seen and expected for analogous distortions involving mechanically-induced director rotation in nematic elastomers, see the experiments of Finkelmann *et al* [18].

B. Additional, non-soft shear relaxation

It is possible to find slightly softer deformation trajectories than that illustrated above by including the yx component of deformation. For systems with clamps allowing changes in the shape of the xy section of the elastomer, or for micro-structures that we will explore below, this extra freedom might be a way of reducing the elastic energy between the two minimal states at $\phi = 0$ and $\phi = \pi$. Thus the deformation gradient and its inverse transpose are respectively

$$\begin{pmatrix} 1 & 0 & \lambda_{xz} \\ \lambda_{yx} & 1 & \lambda_{yz} \\ 0 & 0 & 1 \end{pmatrix} \text{ and } \begin{pmatrix} 1 & -\lambda_{yx} & 0 \\ 0 & 1 & 0 \\ -\lambda_{xz} & \lambda_{yx}\lambda_{xz} - \lambda_{yz} & 1 \end{pmatrix} \quad (5)$$

where, with the aid of the latter, one can confirm that the layer normal has not been rotated nor the layer spacing changed by the imposed deformation. With this greater freedom, the threshold to both director rotation and strain relaxation can be avoided. Thus the free energy cost is lowered from the previous trajectory, see the dotted curve also plotted in Fig. 3(a) for direct comparison with the energy when less relaxation is permitted. This minimal free energy has had the optimal deformation gradients in $\underline{\underline{\lambda}}$ put into f of eqn (2). These components are:

$$\lambda_{xz} = -\frac{r-1}{\rho}\sin\theta\cos\theta(1-\cos\phi) \quad (6)$$
$$\equiv -\Lambda(1-\cos\phi)$$
$$\lambda_{yz} = \Lambda\left(1 - \frac{r-1}{a^2 r}\sin^2\theta\cos\phi\right)\sin\phi \quad (7)$$
$$\lambda_{yx} = \frac{r-1}{2a^2 r}\sin^2\theta\sin 2\phi \quad (8)$$

with the combination $a^2 = \cos^2\phi + (\rho/r)\sin^2\phi \leq 1$. The yx and yz shears plus the accompanying director rotation are plotted in Fig. 4 against the imposed xz shear.

The rotation is straightforwardly $\cos\phi = 1 + \lambda_{xz}/\Lambda$ from (6) and must be inserted into eqns (7) and (8) to get $\lambda_{yz}(\lambda_{xz})$ and $\lambda_{yx}(\lambda_{xz})$. The singular rotation initially and finally is just that of the $\cos^{-1}$ function:

$$\phi = \pm\sqrt{-2\lambda_{xz}/\Lambda} \quad \text{for} \quad \lambda_{xz} \lesssim 0 \quad (9)$$
$$\phi = \pm\sqrt{2(2-\lambda_{xz}/\Lambda)} \quad \text{for} \quad -2\Lambda \lesssim \lambda_{xz} \quad (10)$$

At $\phi = \pi/2$ one has $\lambda_{xz} = -\Lambda$, the xz section of the sample has gone half way between the states of Figs 2(a) and (b).

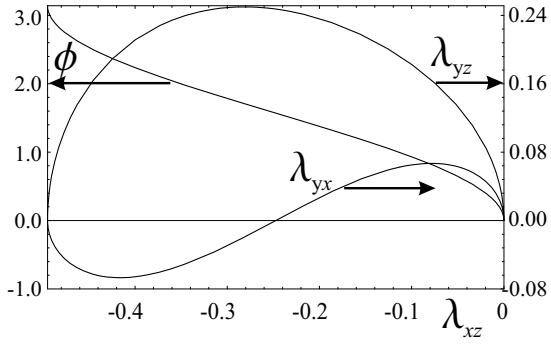

FIG. 4: The yx and yz shears and in-plane director rotation ϕ against imposed shear λ_{xz} for the softer case where yx relaxation is permitted (r and θ as before).

The new shear, yx, is antisymmetric about $\phi = \pi/2$. It must vanish when $\hat{\mathbf{c}}$ points along $\hat{\mathbf{y}}$ since the natural change of the sample would be to elongate along $\hat{\mathbf{y}}$ (which we as yet suppress, $\lambda_{yy} = 1$) and to yz-shear. There is no need for in-plane shape change, $\lambda_{yx} = 0$.

The yz deformation is numerically equal to Λ at $\phi = \pi/2$ as one would expect – when the director has rotated by $\pi/2$ the y axis has the same significance as the x axis initially had. The intermediate state $\phi = \pi/2$ with $\hat{\mathbf{n}}$ in the yz plane and $\hat{\mathbf{c}} = \hat{\mathbf{y}}$, is where there must be maximal yz-distortion due to director rotation and indeed the energy can be seen to be symmetric about $\pi/2$ (actually seen in the plots against λ_{xz} to be symmetric about the value $-\Lambda$). However, since we are dealing with large deformations that do not add linearly, the additional shear introduces an apparent asymmetry about $\phi = \pi/2$ into the form of the yz-relaxation. (In Appendix B, we show that this apparent asymmetry, and more asymmetries to be discussed below, are simply consequences of the geometric need to compound rather than add large deformations.) The yz relaxation reaches a maximum value at $\phi = \frac{1}{2}\cos^{-1}\left[\overline{r-1}\sin^2\theta/\left(\overline{r-1}\cos^2\theta + r + 1\right)\right]$.

The energy maximum offers the same height of barrier between the minimal states as before. With respect to the minimal value of $3\mu/2$, the barrier is $2f_{\rm bar}/\mu = 2(r-1)^2\sin^4\theta/\left[r(r+(r-1)\cos 2\theta)\right]$. As in all expressions involving the energy cost on rotation or shear, it scales as $(r-1)$, that is it vanishes on isotropy ($r = 1$). Otherwise, the energy is somewhat reduced, see the dotted curve in Fig 3(a), but at the expense of a more complex system of sympathetic shears. We now explore a final shear scenario to lower the free energy of distortion still further.

C. Soft deformations

If the rubber has total freedom to shear and distort as the director rotates, then in ideal systems there is zero accompanying rubber elastic cost. The mechanism arises because the distribution of chains is accommodated by

the changing shape of the body without the distribution's distortion and thus with no decrease of the entropy or modification of the liquid crystal order. Such distortions are well-known in nematic elastomers [5] deep into the non-linear regime. They have been explored theoretically in SmC elastomers [9, 11, 12] where the constraint of layers must be rigidly observed. A soft deformation gradient (and its inverse transpose), which leaves the layer normal unrotated and the layer spacing unchanged, is

$$\underline{\underline{\lambda}} = \begin{pmatrix} \lambda_{xx} & 0 & \lambda_{xz} \\ \lambda_{yx} & \lambda_{yy} & \lambda_{yz} \\ 0 & 0 & 1 \end{pmatrix} \tag{11}$$

$$\underline{\underline{\lambda}}^{-T} = \begin{pmatrix} \lambda_{yy} & -\lambda_{yx} & 0 \\ 0 & \lambda_{xx} & 0 \\ -\lambda_{yy}\lambda_{xz} & \lambda_{yx}\lambda_{xz} - \lambda_{xx}\lambda_{yz} & 1 \end{pmatrix} \tag{12}$$

where $\lambda_{zz} = \lambda_{xx}\lambda_{yy} = 1$ from incompressibility, $\mathrm{Det}\left(\underline{\underline{\lambda}}\right) = 1$. The elements of the tensor are:

$$\lambda_{xx} = 1/\lambda_{yy} = a(\phi) \tag{13}$$

$$\lambda_{xz} = \Lambda(-a(\phi) + \cos\phi) \tag{14}$$

$$\lambda_{yx} = \frac{r-1}{2ra}\sin^2\theta\sin 2\phi \tag{15}$$

$$\lambda_{yz} = \Lambda\left(\sin\phi - \tfrac{r-1}{2ra}\sin^2\theta\sin 2\phi\right) \tag{16}$$

A factor $\left(1 - \frac{\rho}{r}\right)$ appearing in the expression derived in [12] has been replaced by the equivalent $(r-1)\sin^2\theta/r$. The same types of shears as in eqn (5) enter, but we allow the elongations and contractions λ_{xx} and λ_{yy} to adjust to the changing natural length in the x and y directions as the polymer chain distribution anisotropy is rotated by ϕ. It is this final element, plus the concomitant further changes to the shears, that allows the deformation to be soft. Fig. 5 shows the xx contraction, and the yx and yz shears against the imposed xz shear.

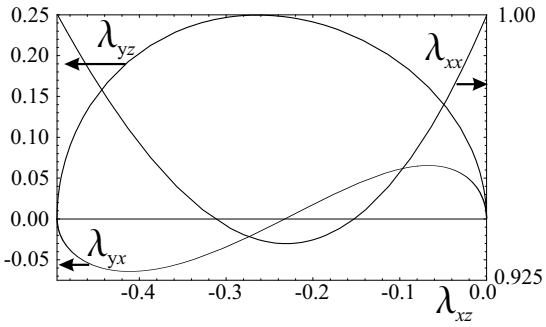

FIG. 5: The yx and yz shears and the xx contraction against imposed shear λ_{xz} for soft deformations (r and θ as before).

In Fig. 6 we show snap shots of an initial cube deforming under a soft $\underline{\underline{\lambda}}$ as the $\hat{\mathbf{c}}$-director advances (right to left) through $\phi = 0$, $\pm\pi/2$, $\pm 2\pi/3$ and $\pm\pi$. It starts from Fig 2(a) and ends in (b), but we are viewing it from along the z axis rather than the y axis.

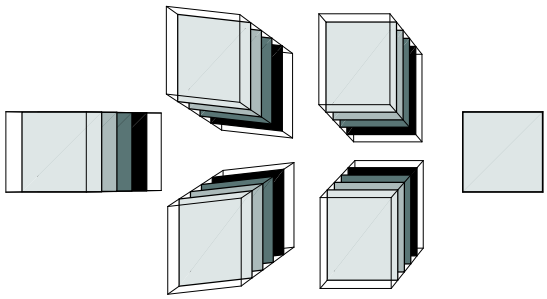

FIG. 6: Soft deformations of a cube of SmC rubber with $r = 8$ and $\theta = \pi/6$ (as before), viewed along the smectic layer normal.

The rotation ϕ is of the singular form as before, with slight modifications that are apparent on comparing the soft $\lambda_{xz}(\phi)$, eqn (14), with the corresponding xz deformation gradient, eqn (6), in the hard case with yx-relaxation. Explicitly, $\phi(\lambda_{xz})$ follows from (14):

$$\phi = \cos^{-1}\left[\frac{r}{\rho}\left(\sqrt{\left(\frac{\rho}{r}\right)^2 + \left(1 - \frac{\rho}{r}\right)\left(\frac{\lambda_{xz}}{\Lambda}\right)^2} + \frac{\lambda_{xz}}{\Lambda}\right)\right] \tag{17}$$

with singular rotation initially (and analogously finally):

$$\phi \sim \pm\sqrt{\frac{2r}{\rho}\lambda_{xz}/\Lambda} \quad \text{for} \quad \lambda_{xz} \lesssim 0. \tag{18}$$

Note that λ_{xz} is no longer $-\Lambda$ when the $\hat{\mathbf{c}}$-director is along $\hat{\mathbf{y}}$, that is $\phi = \pi/2$, but is instead $\lambda_{xz} = -\Lambda\sqrt{\rho/r} \equiv -\Lambda\sqrt{1 - \frac{r-1}{r}\sin\theta\cos\theta}$, a numerically smaller value than before. Figs 2(a) and (b) correspond to shears of 0 and -2Λ and when the system has $\phi = \pi/2$ it is geometrically half way between. The *apparent* inconsistency because the shear is not $-\Lambda$, is again a consequence of nonlinearity, see Appendix B. However, when the $\hat{\mathbf{c}}$-director is transverse, there is, as expected, no in-plane shape change, $\lambda_{yx} = 0$, as can be seen in (15) for this ϕ. The yz-shear can be seen to be Λ at $\phi = \pi/2$, but since $\lambda_{xz} > -\Lambda$ there, then $\lambda_{yz}(\lambda_{xz})$ is asymmetric about $-\Lambda$, for the same reasons as above.

III. SAMPLE GEOMETRY AND TEXTURED RESPONSE

The form of deformation in response to an imposed shear λ_{xz} or director rotation ϕ (driven perhaps electrically) will depend on what components of $\underline{\underline{\lambda}}$ are inhibited by geometrical constraints. We now discuss different sample geometries. Hiraoka *et al* [4] created monodomains and observed large spontaneous shears on the SmA → SmC transition in a sheet geometry, Fig. 7(a), where the y dimension of the sample is small. Alternatively smectic actuation, albeit of electroclinic effects in SmA*

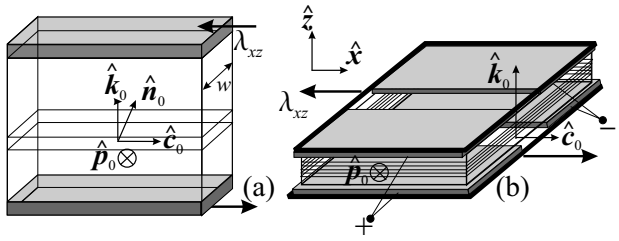

FIG. 7: (a) Sheet and (b) Slab geometries for SmC elastomers. Rigid clamps (shaded) are shown on the xy sample surfaces. λ_{xz} shear displacements are indicated by arrows. A few smectic planes are indicated in each case, with normals $\hat{\mathbf{k}}_0$. Polarisation $\mathbf{P}$ in the y direction (of extent w) emerges from the xz sample surfaces. Lines of electric flux in the slab case are captured by enveloping the small xz surfaces by overhanging, split xy electrodes, their charge being identified by $\pm$.

elastomers where tilt and shear are purely electrically-driven, has been achieved [19] with small shears in the slab geometry of Fig. 7(b), a geometry that is also highly interesting for SmC elastomers. In each case the sample is effectively held by rigid clamps in the xy plane – actually tape overlapping the sheet sample, and by glass plates in the slab case. We expect changes in the polarisation, $\mathbf{P}$ to be along $\hat{\mathbf{y}}$ and hence suitable flexible electrodes would be needed for detection of charges on the xz faces for the sheet sample. In the slab case, rigid xy electrodes under the plates are suggested for detecting xz surface charges.

The clamps in each case eliminate λ_{xx} and λ_{yy} in their vicinity. For sheets this constraint is over a small fraction of the sample. The variation of λ_{xx}, say, in the z direction away from the boundaries to more favourable bulk values is slow, thus generating (by compatibility) minor λ_{xz} additions to the deformation. Under these circumstances one could expect elastically the sheet deformations to be of the soft form eqn (11) where the additional freedom gives a much reduced energy cost. By contrast, the slab geometry imposes a constant $\lambda_{xx} = 1$ throughout because the sample is thin. Slabs then could at best have the distortion eqn (5) where the diagonal elements are all 1. Analogously, rigid xy plates would suppress in their vicinity any λ_{yx} shear. It is possible that in the bulk of slabs λ_{yx} is suppressed, though z-variation of λ_{yx} generates through compatibility λ_{yz} which we are already considering and it is possible that even for slabs, in the bulk one must consider $\lambda_{yx} \neq 0$.

In both sheets and slabs, imposing λ_{xz} induces macroscopic translations in the y direction resulting from the accompanying λ_{yx} and λ_{yz} shears. Either the rigid plates are constrained to move only in the x direction, or because if y displacements were to develop, then there would be counter-torques from the applied x-forces which would resist this y-displacement. However, such shears drastically reduce the energy, and the conflict between their development and the action of torques is overcome by the development of microstructure or textures of bands of shears of alternating sign, corresponding to rotations of alternating sign, $\pm\phi$, but with the same λ_{xz}. At the macroscopic level the λ_{ij} components that are odd in ϕ cancel with each other, and those even in ϕ add. Thus a body, with $\pm\phi$ shears in equal proportions, as a whole would have a deformation gradient of the form:

$$\underline{\underline{\lambda}}_{\rm mac} = \begin{pmatrix} \lambda_{xx} & 0 & \lambda_{xz} \\ 0 & \lambda_{yy} & 0 \\ 0 & 0 & 1 \end{pmatrix} \tag{19}$$

even though locally $\lambda_{yx}(\pm\phi) \neq 0$ and $\lambda_{yz}(\pm\phi) \neq 0$. They ensure no macroscopic, constraint-violating, $\hat{\mathbf{y}}$-displacements develop across the sample. Such textures will be required for all three deformations we have explored, soft or non-soft. The development of microstructure is analogous to that in the soft deformations of nematic elastomers where the underlying soft deformations are observed, but where necessary in textures to allow the underlying soft response to occur [20]. Texture is not the cause of softness, but a symptom that arises from softness in the presence of constraints.

The reader can see a concrete example of $\underline{\underline{\lambda}}_{\rm mac}$ by putting, say, the $\phi = \pi/2$ body on top of that with $\phi = -\pi/2$. (At this special ϕ, this picture is close to that in Fig. 8 below.) Looking at the position of the overall top xy-surface with respect to that of the bottom, it is clear that there has been a xz-shear, but that overall there is no y-relative displacement and thus overall no λ_{yz}. What is important is that the bodies are placed on top of each other, rather than in any other configuration, a question of textures to which we turn below. With the above $\underline{\underline{\lambda}}_{\rm mac}$ the energy will have been reduced (to zero in the ideal soft case) and yet overall the body has conformed to boundary conditions that are inconsistent with the underlying deformations (4), (5) and (11). The development of textures to achieve soft response in the face of incompatible boundary conditions quasi-convexifies the free energy, a process well-understood in Martensite [13], and in nematic elastomers [6, 14]. It is important in the response of the constrained samples that we are studying here.

We now derive the full form of the textures that arise for the two geometries that do not rotate the smectic layer normals. We limit ourselves to such textures since then the xy sample faces can then retain their orientation as deformation proceeds.

A. Forms of textures

Neighbouring laminates in a texture with deformations $\underline{\underline{\lambda}}_{\pm\phi}$ that are in contact through a common surface must suffer deformations that are rank-one connected [13], otherwise there is a geometric inconsistency between the specification of translations of their interfacial elements by

$\underline{\underline{\lambda}}_{+\phi}$ and $\underline{\underline{\lambda}}_{-\phi}$, that is:

$$\underline{\underline{\lambda}}_{+\phi} - \underline{\underline{\lambda}}_{-\phi} = \mathbf{a} \otimes \mathbf{s} \tag{20}$$

$$= 2 \begin{pmatrix} 0 & 0 & 0 \\ \lambda_{yx} & 0 & \lambda_{yz} \\ 0 & 0 & 0 \end{pmatrix} \tag{21}$$

since $\lambda_{yx}(\phi)$ and $\lambda_{yz}(\phi)$ are both odd about $\phi = 0$ whereas $\lambda_{xz}(\phi)$, $\lambda_{xx}(\phi)$ and $\lambda_{yy}(\phi)$ are even. Here $\mathbf{a}$ is a vector in a laminate's surface in the target state and $\mathbf{s}$ is the surface normal of a laminate back in the reference state, that is the normal to the boundary of a region that will transform into a laminate. It is straightforward to see that (uniquely) $\mathbf{a} = (0, 1, 0)$ and $\mathbf{s} \propto (\lambda_{yx}, 0, \lambda_{yz})$. As the textures evolve with ϕ, they have normals in the zx plane and, if they rotate at all with changing ϕ, it is about the y axis. The texture normal in the target space is given by the usual transformation for normals of planes embedded in an elastic solid, $\mathbf{s}' = \underline{\underline{\lambda}}_{\phi}^{-T} \cdot \mathbf{s}$.

For the simple deformation eqn (4) with $\lambda_{yx} = 0$, the normal is $\mathbf{s} = \mathbf{s}' \propto (0, 0, \lambda_{yz})$. Thus the textures and the smectic layers share the unchanging normal $\mathbf{s}' = \hat{\mathbf{k}}_0 = \hat{\mathbf{z}}$, Fig. 8. Successive xy slices of the solid suffer alternating

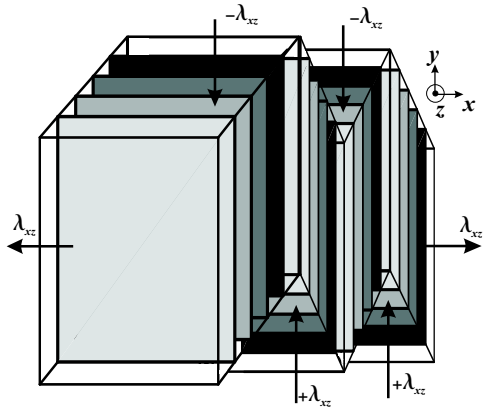

FIG. 8: A slice through a solid deforming with a textured version of (4) for $\underline{\underline{\lambda}}$. Alternating $\pm\lambda_{yz}$ shears lead to no overall macroscopic λ_{yz} but to the desired imposed λ_{xz}.

λ_{yz} transverse shears. This pattern is a possibility for slab geometries, but less likely for sheets where a soft texture is a possibility we examine below. There is no question of polarisation charges residing on the internal surfaces of this texture since $\mathbf{P}$ rotates in the plane of the laminates and is never sliced by the internal interfaces.

For both the other choices of deformation, $\mathbf{s}'$ has a universal form from letting the appropriate $\underline{\underline{\lambda}}^{-T}$ act on $\mathbf{s}$ that is independent of softness or not:

$$\mathbf{s}' \propto (\lambda_{yy}\lambda_{yx},\ 0,\ \lambda_{yz} - \lambda_{yy}\lambda_{yx}\lambda_{xz}) \tag{22}$$

$$\rightarrow (\sin\theta\cos\phi,\ 0,\ \cos\theta) \tag{23}$$

whence the texture normal has an angle, χ, to the z axis:

$$\chi(\phi) = \tan^{-1}\left[\cos\phi \tan\theta\right]. \tag{24}$$

As the $\hat{\mathbf{c}}$-director rotates around $\hat{\mathbf{k}}_0$, the normal to the textures rotates about the $\hat{\mathbf{y}}$ axis, Fig. 9, with $\chi = 0$ for $\phi = \pi/2$, that is $\mathbf{s}'$ is along $\hat{\mathbf{k}}_0$

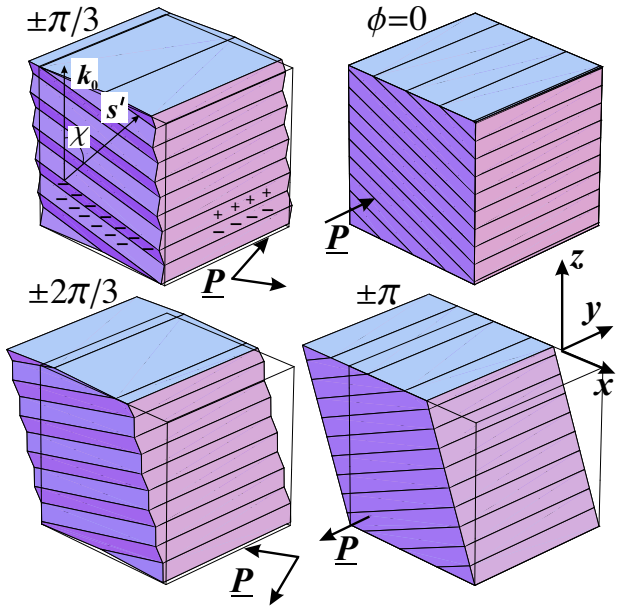

FIG. 9: An initially cubic sample deforming softly with laminates of yx and yz shears of alternating sign and with xz shear advancing from 0 to -2Λ in steps of $\pm\pi/3$ in director rotation ϕ (marked on figures) about the z axis. The alternating shear deformations lead to no corresponding macroscopic shears whereas the imposed λ_{xz} does. The laminate normal $\mathbf{s}'$ is shown for the example of $\phi = \pi/3$. It starts and finishes parallel to $\hat{\mathbf{n}}$ but in general makes an angle χ with the layer normal $\hat{\mathbf{k}}_0$ given in the text. The deformations away from the initial shape (light reference frame given in $\phi \neq 0$ pictures) reveal the slight contraction λ_{xx} along x and a compensatory lengthening along y, see e.g. $\phi = \pi/3$, for $\phi \neq 0, \pm\pi$. The $\pm\pi/2$ case is like Fig 8, that is with $\chi = 0$, but with $\lambda_{xx}, \lambda_{yy} \neq 1$.

Our analysis of soft modes and non-soft modes with yx-relaxation, has been based upon the free rotation of the normal of the system of laminates about the y axis. It is possible that the motion of the laminate surfaces, through the assembly of smectic layers that is stationary, is in fact pinned. A rubber is liquid-like at the molecular level, accounting for the extreme extensibility of rubbers and, for instance, their motionally-narrowed NMR lines. It is known that laminates evolve and rotate easily in nematic elastomers responding at low energy cost [20]. It is conceivable that textures in Smectic C elastomers are not pinned and that low-energy deformations are thus possible as we propose. Experiment is vital to determine whether pinning is active or not.

Another uncertainty is the energy cost of laminate walls. The directors on opposite sides of a laminate surface are rotated to $\pm\phi$. At $\phi = \pi/2$ the layers and laminates share a common normal and laminate surfaces are a π twist wall. At other values of ϕ, the laminates and

layers are oblique to each other and the wall is complicated. In any event there is a cost to walls. This cost, when weighed against the cost of not conforming to constraints, will determine the fineness of textures. This question is addressed in the literature for nematic elastomers — we do not pursue it here.

One final, trivial but perhaps important form of texture remains, a simple disproportionation that might occur in both slab and sheet geometries where the top portion of the sample is xz-sheared to its maximum soft extent -2Λ and the bottom portion is in an equally low energy, undistorted state, see Fig. 10. The two states are

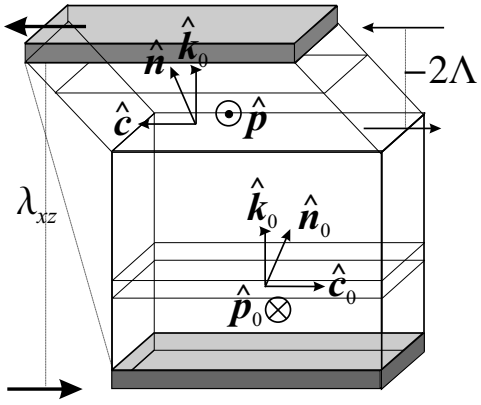

FIG. 10: A sample deforming by disproportionation. The macroscopic λ_{xz} shear displacements are indicated by heavy arrows and consists of a fraction of undistorted sample and the complementary fraction distorted by -2Λ.

separated by a π twist wall. It is possible that a sample might deform this way if rotations of textures are pinned and if the energy cost of laminate interfaces discussed above is too high. Only one, non-rotating interface is required for this mode of deformation. Simple geometrical considerations determine the volume fraction Φ of sample that is transformed into the $\phi = \pi$, $\lambda_{xz} = -2\Lambda$ state: $\Phi = \lambda_{xz}/(-2\Lambda)$. A particularly simple ferro-electric response arises, as we see in the next section.

IV. FERRO-ELECTRIC RESPONSE

When a polarisation $\mathbf{P}$ is sliced by a surface, by Gauss's theorem a surface charge density $\sigma = -\Delta P_\perp$ develops that is equal to the change of the normal component of $\mathbf{P}$ from one side to the other. Thus at the xz surfaces of both sample geometries, $\sigma^{(xz)} = P\cos\phi \equiv P_y$, which we now relate to imposed deformation λ_{xz}.

The non-soft deformation with a threshold has singular director rotation against imposed λ_{xz} because it too is essentially of the $\cos^{-1}$ form that subsequent deformation modes are also shown to be. Between λ_1 and λ_2, the variation is almost indistinguishable from $\cos\phi = (2\lambda_{xz} - \lambda_1 - \lambda_2)/(\lambda_1 - \lambda_2)$ where λ_1 and λ_2 are the thresholds to director rotation that arise in this constrained case. Thus the surface charge evolves linearly with λ_{xz}:

$$\sigma^{(xz)} = -P(2\lambda_{xz} - \lambda_1 - \lambda_2)/(\lambda_1 - \lambda_2). \qquad (25)$$

For the non-soft deformation without a threshold, eqn (5), one sees directly from eqn (6) that the xz-surface charge density is:

$$\sigma^{(xz)}(\lambda_{xz}) = -P(1 + \lambda_{xz}/\Lambda). \qquad (26)$$

Recall that the imposed shear λ_{xz} varies from 0 to -2Λ and thus this surface charge reverses linearly with the applied shear deformation. It would not change any further, were the shear to be increased beyond -2Λ.

When deformation is soft, the connection between $\cos\phi$ and λ_{xz} is slightly more complicated, despite being linear at the start and end of the rotation. Eqn (17) gives the explicit shear-dependence:

$$\sigma^{(xz)}_{\rm soft} = -P\frac{r}{\rho}\left(\sqrt{\left(\frac{\rho}{r}\right)^2 + \left(1 - \frac{\rho}{r}\right)\left(\frac{\lambda_{xz}}{\Lambda}\right)^2} - \frac{\lambda_{xz}}{\Lambda}\right). \qquad (27)$$

A. Charging of laminate surfaces; overall electrostatic energy and mechanical stability

For the non-trivial textures with the laminate normals not along the layer normals, the polarisation is sliced by the internal surfaces separating laminates in the texture. One must then consider the energies of the resulting internal surface charge distributions in both the cases of sheets and slabs. The layer normals $\mathbf{s}'$ rotate about y in the xz plane. The y-component of $\mathbf{P}$, giving rise to the xz-external surface charges discussed above and pictured in Figs. 2 and 7, does not contribute to the internal sheets of charge, which arise rather from the P_x component intersecting the laminate surfaces, that is $\sigma_{\rm lam} \propto P\hat{\mathbf{x}}\cdot\mathbf{s}'$. The internal surface charge density is therefore

$$\frac{\sigma^{\rm lam}}{P} = \pm\sin\phi\sin\chi = \pm\tfrac{1}{2}\frac{\tan\theta\sin 2\phi}{(1+\tan^2\theta\cos^2\phi)^{1/2}}. \qquad (28)$$

One must ask then whether these charges have a significant energetic effect?

In the sheet geometry relatively little of the otherwise uniform field generated by the xz-sheets of external surface charge leaks out of the sample. The y-internal electric displacement in the sample is $D^{\rm int}_{(y)} = \sigma^{(xz)} = -P\cos\phi$. If the textures are fine, the electric displacement between internal surfaces of alternating charge is also not lost, and is $D^{\rm lam}_{s'} = P\sin\phi\sin\chi$, from eqn (28). This D is in the $\pm s'$ directions. Finally the component of P_x that is in the plane of the laminates intersects the external yz-surfaces and generates $\sigma^{(yz)}$ external surface charge densities, see Fig. 11. These are $\sigma^{(yz)} = -P\sin\phi\cos\chi$ and change sign between ends of

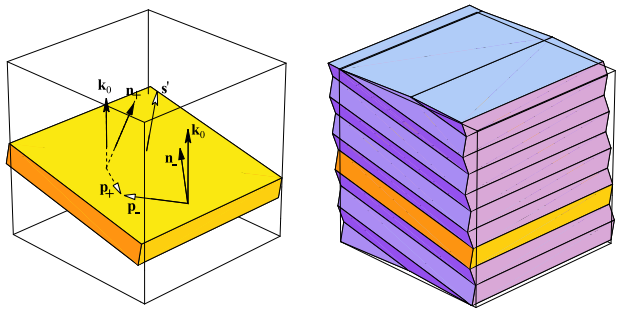

FIG. 11: Surface charge density on the xz and yz surfaces of an elastomer deformed so that the director has rotated by $\pi/3$. One laminate is shown with the polarization vector $\mathbf{P}$ (in the xy plane) cutting its internal surfaces from within, and from the laminate above where $\mathbf{P}$ has rotated oppositely around z. The lower surface of the laminate is cut in the opposite sense and hence the surface charge is opposite.

neighbouring laminates as $\phi \to -\phi$. The charges generate small effective internal fields because the yz surfaces are small, are widely separated in the sheet geometry and, in any event, are oppositely charged in stripes, so we can ignore their energetic effect. At the exceptional points $\phi = \pm\pi/2$, the internal fields $E^y_{\rm int} = 0$ and $E_{\rm lam} = 0$, the latter because the laminate normals are along the layer normals z. All the surface charges are confined to the yz external surfaces which we have just argued generate an internal field that we can ignore. The overall electrostatic energy density, $f_{\rm el}$, from internal fields depends in part on the anisotropic dielectric tensor of the elastomer which we represent for simplicity, see appendix C, by a single averaged value ϵ:

$$\begin{aligned} f_{\rm el} &= \tfrac{1}{2}\frac{P^2}{\epsilon\epsilon_0}\left\{\cos^2\phi + \sin^2\phi\sin^2\chi\right\} \\ &= \tfrac{1}{2}\frac{P^2}{\epsilon\epsilon_0}\cos^2\phi/\left(\cos^2\theta + \sin^2\theta\cos^2\phi\right). \end{aligned} \quad (29)$$

There is a weak χ-dependence in $1/\epsilon$ that we estimate in Appendix C and argue that we can neglect in the estimates below.

At first sight this energy is perhaps alarming. $f_{\rm el}$ is maximal, $f_{\rm el} = P^2/(2\epsilon\epsilon_0)$ at $\phi = 0, \pm\pi$ and is minimal, $f_{\rm el} = 0$, at $\phi = \pm\pi/2$. For soft deformations, where there is no elastic cost, the director should spontaneously rotate to $\phi = \pm\pi/2$ and the sample should spontaneously shear to $-\Lambda$. It is likely however that the xz external surfaces, that are initially charged, attract counter-ions from their surroundings and are neutralised. There is accordingly no electrostatic cost at $\phi = 0$ (and finally at $\phi = \pm\pi$) since no internal field $E^y_{\rm int}$ is generated. The only internal fields are those between successive (internal) laminate surfaces (unless these too are neutralised by internal conduction processes). The electrostatic energy density is then simply:

$$f'_{\rm el} = \frac{P^2}{\epsilon\epsilon_0}\frac{\sin^2 2\phi\sin^2\theta}{\cos^2\theta + \sin^2\theta\cos^2\phi}. \quad (30)$$

There is thus no electrostatic cost at $\phi = 0, \pm\pi/2, \pm\pi$. All these points are local minima of the free energy and cost in deviating from these points means that spontaneous rotation is avoided. It does suggest however that there is a complex energy associated with the path between $\lambda_{xz} = 0$ and -2Λ for softly deforming elastomers. Should the deformation be of the hard type with $\lambda_{yx} \neq 0$ which demands complex textures as in the soft case, then the elastic energy has to be added to the electrostatic energy $f'_{\rm el}$, the resultant of which depends on the relative scale of rubber elastic and ferro-electric energies.

Values of P for smectic C* systems are in the range $10^{-5} - 10^{-4}$C/m^2. One must compare the resulting energy density with elastic energy densities in the problem which are $\frac{1}{2}\mu 10^{-2}$, taking the strain energy at the maximal (barrier) value, 10^{-2} in units of $\mu/2$, see Fig. 3(a). For $\mu \sim 10^5$J/m^3 this puts the ratio of the electro-static to elastic energies in the range 10^{-2} to 1 – under some circumstances electrostatics may be important, making the need for experimental results still greater to discern the different mechanisms that will be selected by these competitive energies. It is possible that one might have complicated free energies of deformation that result from the sum of the elastic and electrostatic influences.

Slabs would appear to have the choice of hard deformations with or with out the additional yx shear relaxation. Without yx shears, the laminate normals are along the layer normals and hence always perpendicular to the polarisation that rotates about the z axis as ϕ evolves. Accordingly, no internal sheets of charge develop for intermediate imposed shears. With yx shears the laminate surfaces have normals as in the soft case and the same internal surface charges are generated. If the texture is fine, the distance between alternating internal sheets of charge is small and little of the associated field leaks out. Then there would be an energetic cost as for laminates discussed above.

The charges on the xz and yz external surfaces give rise to fields that largely leak out of the sample and hence again we ignore their contribution to the energy. The leaking field lines from the xz surfaces can be captured by overhanging electrodes as in Fig 7(b) and hence the surface charge, and P, can be measured.

B. Electrically driven actuation?

The inverse response when applying a potential to elastomers in the two geometries in order to generate a shear strain also needs quantifying. Elastic barriers to deformation still exist, but now one is coupling external potentials to the charge layers that exist on the free surfaces, that is achieving an energy change per

unit xz-area of sample of $\frac{1}{2}\sigma V$ on achieving $\sigma = 0$ as a result of applying a voltage V across the sample and mechanically switching as far as the maximum in the elastic energy barrier (where $\phi = \pi/2$). For the favourable case of the sheet, taking $V = 100$ and thickness $w = 10^{-3}$m, the relative energy densities (electrical to elastic) are $VP/(w\mu 10^{-2}) \sim 10^{-2}$ even for the larger values of P. The reason is that internal electrical fields that set the scale of energies above are $E_{\rm int} \sim 10^7$V/m, much larger than those typically able to be applied here. One must conclude that elastomers offer little hope of electro-mechanical actuation for their very large potential strains, except perhaps in extreme forms of the sheet geometry and with large fields (ie thin samples).

C. Experimental observations

The internal fields, that we argue could play a significant role in fixing the mechanical stability of these elastomers in their textured state, are perhaps open to direct observation that might help determine what rotations are accompanying shears. These intense fields are given, see Appendix C, by $\mathbf{E} = \frac{1}{\epsilon_0}\underline{\underline{\epsilon}}^{-1} \cdot \mathbf{D}$ with $\mathbf{D} = P_{s'}\mathbf{s}'$ the electric displacement generated by the internal surface charges and directed along the laminate normals. Thus $E_i = \frac{1}{\epsilon_0}\epsilon^{-1}_{is'}D_{s'}$. The field is not purely along the laminate normal because this direction is not a principal direction of the dielectric tensor. Guest species with for instance characteristic absorption or florescence could be aligned with the field rather than with, say, the director or smectic layer normal. In particular a distinction between the field and director directions emerges as soon as rotation starts and would be an independent check of the development of microstructure. Absorption or florescence probes suggested above are invariant under $\mathbf{s}' \to -\mathbf{s}'$ and thus would not find the alternating texture structure nugatory. It is likely that the choice of geometry, slab or sheet, will yield very different results.

V. CONCLUSIONS

The deformation path taken by a smectic-C elastomer in having the direction of its spontaneous polarization mechanically reversed is calculated for slab and sheet geometries. Different possible textures result according to geometry, the constraints at surfaces, the elastic shear energy and the charging of internal texture surfaces when they cut the polarization. The relative roles of polarization and elastic cost is a matter that we believe is still most open and experiments are urgently required.

Acknowledgement We are grateful to Prof. K. Bhattacharya for pointing out the necessity to examine the effect of charges on internal surfaces that led to the analysis of section IV A.

APPENDIX A: ENERGY SCALE μ FOR DEFORMATIONS

We model smectic elastomers as essentially nematic elastomers with strong constraints of layering. Thus μ that scales the underlying rubber elastic energy would be the shear modulus for the rubber, were it able to enter its isotropic state. More usefully one can relate it to certain shear or extensional moduli in the SmC elastomeric state. Elongation along the $\hat{\mathbf{c}}_0$ direction, $\lambda_{xx} > 1$, or shear with displacement in the positive x direction, $\lambda_{xz} > 0$, both do not rotate the $\hat{\mathbf{c}}$-director, provided the layer normal $\hat{\mathbf{k}}_0$ is fixed (for instance by clamps or rigid plates). We are assuming rigid Sm order – for instance elongations are accompanied by $\lambda_{yy} = 1/\lambda_{xx}$ since contraction along z is forbidden (it would alter the layer spacing) and these deformations are two-dimensional as in the case of SmA elastomers undergoing similar strains [7] and which have been modelled in these terms [8]. Without rotations and other shears, the free energy cannot drastically reduce, as in the rest of this investigation. The free energies of such distortions are:

$$\begin{aligned} f(\lambda_{xz} \geq 0) &= \tfrac{1}{2}\mu\left(3 + \frac{1}{4r}\left[r + 1 + (r-1)\cos 2\theta\right]^2 \lambda_{xz}^2\right) \\ f(\lambda_{xx} \geq 1) &= \tfrac{1}{2}\mu\left(\frac{(\lambda_{xx}-1)^2}{8r}\left[r^2 + 1 - (r-1)^2\cos 4\theta\right]\right. \\ &\quad \left. + \frac{1}{4\lambda_{xx}^2}\left[4 + 3\lambda_{xx}^2 + 2\lambda_{xx}^3 + 3\lambda_{xx}^4\right]\right) \end{aligned}$$

with corresponding small strain moduli:

$$\begin{aligned} k_{xz} &= \frac{\mu}{4r}\left[r + 1 + (r-1)\cos 2\theta\right]^2 \\ k_{xx} &= \frac{\mu}{8r}\left(1 + 30r + r^2 - (r-1)^2\cos 4\theta\right) \end{aligned}$$

A sense of how much easier deformation is with relaxation can be seen in Fig. 12. The moduli, along with the spontaneous distortion (or limits to softer deformation and completion of charge switching) and conoscopy (for θ) give experimental insight into μ, $r-1$ and $\cos\theta$.

APPENDIX B: NON-LINEARITY AND APPARENT ASYMMETRIES IN DEFORMATIONS

The deformation (5) leads to a λ_{yz} apparently asymmetric about $\phi = \pi/2$, or equivalently $\lambda_{xz} = -\Lambda$. Manifestly when $\hat{\mathbf{c}}$ has been rotated to $\hat{\mathbf{y}}$, the yz shear is geometrically maximal and should reverse to zero as $\phi \to \pi$ just as it advanced while $\phi \to \pi/2$. We demonstrate that the failure of (7) and Fig. 4 to exhibit symmetry about $\lambda_{xz} = -\Lambda$ is only apparent. It is a consequence of geometrical non-linearity (the need to compound rather than add finite deformations).

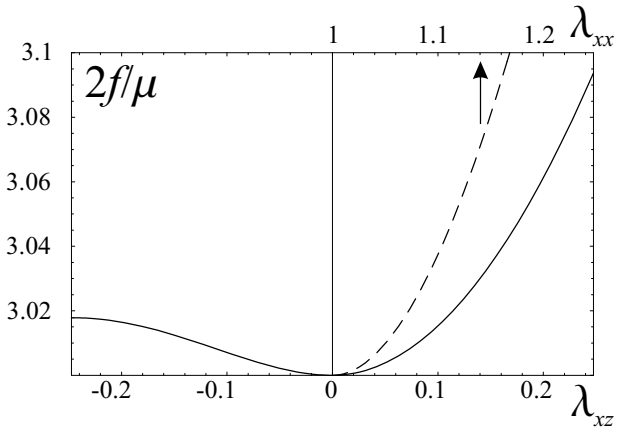

FIG. 12: Energy of deformation for both positive (hard) and negative (softer) shear λ_{xz}, and for extensions $\lambda_{xx} \geq 1$ (dotted, upper scale) up to strains of $\pm\Lambda = \pm 0.246$, for the values of r and θ adopted in the text. Note how much lower the energy of distortion is if sympathetic relaxations and director rotation are permitted.

Consider deformed states of the solid at $\phi = \pi/2 + \zeta$. One can compound deformations:

$$\underline{\underline{\lambda}}_{\phi} = \underline{\underline{\lambda}}'_{\zeta} \cdot \underline{\underline{\lambda}}_{\frac{\pi}{2}}$$

where $\underline{\underline{\lambda}}_{\phi}$ and $\underline{\underline{\lambda}}_{\frac{\pi}{2}}$ (unprimed tensors) are with respect to the original reference state, $\mathbf{X}^0$ say, while $\underline{\underline{\lambda}}'_{\zeta}$ is a deformation gradient with respect to the reference state $\mathbf{X}'$ resulting from the deformation $\underline{\underline{\lambda}}_{\frac{\pi}{2}}$, that is $\mathbf{X}' = \underline{\underline{\lambda}}_{\frac{\pi}{2}} \cdot \mathbf{X}^0$. For (5), $\underline{\underline{\lambda}}_{\frac{\pi}{2}}$ and $\underline{\underline{\lambda}}'_{\zeta}$ are respectively:

$$\begin{pmatrix} 1 & 0 & \Lambda \\ 0 & 1 & \Lambda \\ 0 & 0 & 1 \end{pmatrix} \quad \begin{pmatrix} 1 & 0 & \lambda'_{xz} \\ \lambda'_{yx} & 1 & \lambda'_{yz} \\ 0 & 0 & 1 \end{pmatrix}.$$

In $\underline{\underline{\lambda}}'_{\zeta}$ one has λ'_{xz} and λ'_{yx} odd and λ'_{yz} even. The roles of x and y in shears involving z have been interchanged in this reference state for $\underline{\underline{\lambda}}'$ with $\hat{\mathbf{c}}$ initially along $\hat{\mathbf{y}}$, just as it was initially along x for the reference state of $\underline{\underline{\lambda}}$. Important for this argument is that rotations of $\pm\zeta$ are physically equivalent.

Consider the difference $\underline{\underline{\Delta\lambda}}$ in the $\underline{\underline{\lambda}}_{\frac{\pi}{2}+\zeta}$ and $\underline{\underline{\lambda}}_{\frac{\pi}{2}-\zeta}$ tensors — it will expose any asymmetry in $\underline{\underline{\lambda}}$ about the $\lambda_{xz} = -\Lambda$ point.

$$\begin{aligned} \underline{\underline{\Delta\lambda}} &= (\underline{\underline{\lambda}}'_{\zeta} - \underline{\underline{\lambda}}'_{-\zeta}) \cdot \underline{\underline{\lambda}}_{\frac{\pi}{2}} \\ &= 2 \begin{pmatrix} 0 & 0 & \lambda'_{xz}(\zeta) \\ \lambda'_{yx}(\zeta) & 0 & 0 \\ 0 & 0 & 0 \end{pmatrix} \cdot \begin{pmatrix} 1 & 0 & \Lambda \\ 0 & 1 & \Lambda \\ 0 & 0 & 1 \end{pmatrix} \\ \Delta\lambda_{yz} &= -2\lambda'_{yx}(\zeta)\Lambda \neq 0 \end{aligned}$$

The extra, yx, relaxation permitted in (5) has created an asymmetry in λ_{yz} about $\pi/2$ that is not a reflection of the true symmetry about $\phi = \pi/2$ that exists in yz shear. We used in the λ'_{yz} this very symmetry with respect to the $\phi = \pi/2$ state. Likewise in (11), allowing further additional elements in $\underline{\underline{\lambda}}$ introduces further geometrical non-linearity. The energy however remains symmetric about $\lambda_{xz} = -\Lambda$, as expected.

APPENDIX C: ELECTROSTATIC ENERGY FROM INTERNAL FIELDS.

The laminate surface charge densities are $\sigma^{\rm lam} = -\Delta P_{s'}$ which generate the displacement fields $D_{s'} = \sigma^{\rm lam}$. The electric field energy density is $\frac{1}{2}\mathbf{D}\cdot\mathbf{E}$ with $\mathbf{E} = \frac{1}{\epsilon_0}\underline{\underline{\epsilon}}^{-1}\cdot\mathbf{D}$. From this expression and given that $\mathbf{D}$ is in the $\mathbf{s}'$ direction, it is clear for the energy that we need the element $\left(\underline{\underline{\epsilon}}^{-1}\right)_{s's'}$ that in eqn 29 and thereafter we have denoted by $1/\epsilon$:

$$f_{\rm el} = \frac{1}{2\epsilon_0} D_{s'} \epsilon^{-1}_{s's'} D_{s'} \qquad \text{(C1)}$$

(no summation over s').

One can make various approximate estimates of the relevant element. One assumption would be to take $\underline{\underline{\epsilon}}$ to be uniaxial about the director $\hat{\mathbf{n}}$. We have already made a similar assumption with the $\underline{\underline{\ell}}$ tensor. However the SmC* phase is anything but uniaxial in its electrical properties – it has ferro-electric ordering along the in-plane direction perpendicular to $\mathbf{c}$. However, one could take the view that the ferro-electric ordering is sterically-driven and remains rigid in the face of internal fields. If one then is examining dielectric effects that result from the polarization of the liquid crystal in the more conventional sense, then perhaps the uniaxial assumption is not so strange as may seem at first sight. In this event, one can characterize $\underline{\underline{\epsilon}}$ by $\epsilon_{\|}$ along $\hat{\mathbf{n}}$ and $\epsilon_{\perp}$ in the directions perpendicular to $\hat{\mathbf{n}}$. In this frame, one can write $\underline{\underline{\epsilon}}$ simply and then extract the element required for (C1):

$$\underline{\underline{\epsilon}}^{-1} = \left(\frac{1}{\epsilon_{\|}} - \frac{1}{\epsilon_{\perp}}\right)\hat{\mathbf{n}}\,\hat{\mathbf{n}} + \frac{1}{\epsilon_{\perp}}\underline{\underline{\delta}} \qquad \text{(C2)}$$

$$\left(\underline{\underline{\epsilon}}^{-1}\right)_{s's'} = \frac{1}{\epsilon_{\perp}} + \left(\frac{1}{\epsilon_{\|}} - \frac{1}{\epsilon_{\perp}}\right)(\hat{\mathbf{n}}\cdot\mathbf{s}')^2 \qquad \text{(C3)}$$

with $\hat{\mathbf{n}}\cdot\mathbf{s}' = \cos\theta\cos\chi + \sin\theta\sin\chi\cos\phi$. Rearrangement with the aid of eqn (24) gives $\hat{\mathbf{n}}\cdot\mathbf{s}' = \cos\theta\sec\chi$. This expression and further use of eqn (24) reduces (C3) to:

$$\left(\underline{\underline{\epsilon}}^{-1}\right)_{s's'} = \frac{1}{\epsilon_{\perp}} + \left(\frac{1}{\epsilon_{\|}} - \frac{1}{\epsilon_{\perp}}\right)(\cos^2\theta + \sin^2\theta\cos^2\phi). \qquad \text{(C4)}$$

Thus the element denoted by $1/\epsilon$ in our energy expressions has some ϕ-dependence, but it is weak compared with the dependence we concentrate on when calculating the energy.

[1] R. B. Meyer, L. Liebert, L. Strzelecki, and P. Keller, J. de Phys. Lett. **36**, L69 (1975).
[2] N. Clark and S. Lagerwall, Appl. Phys. Letts. **36**, 899 (1980).
[3] S. Lagerwall, Ferroelectrics **301**, 15 (2004).
[4] K. Hiraoka, W. Sagano, T. Nose, and H. Finkelmann, Macromolecules **38**, 7352 (2005).
[5] I. Kundler and H. Finkelmann, Macromol. Rapid Commun. **16**, 679 (1995).
[6] M. Warner and E. Terentjev, Liquid Crystal Elastomers (Oxford University Press, Oxford, 2003).
[7] E. Nishikawa and H. Finkelmann, Macromol. Chem. Phys. **200**, 312 (1999).
[8] J. M. Adams and M. Warner, Phys. Rev. E **71**, 021708 (2005).
[9] O. Stenull and T. C. Lubensky, Phys. Rev. Lett. **94**, 018304 (2005).
[10] J. M. Adams and M. Warner, Phys. Rev. E **73**, 031706 (2006).
[11] O. Stenull and T. C. Lubensky, Phys. Rev. E **74**, 051709 (2006).
[12] J. M. Adams and M. Warner, Phys. Rev. E **72**, 011703 (2005).
[13] K. Bhattacharya, Microstructure of martensite (Oxford University Press, Oxford, 2003).
[14] S. Conti, A. DeSimone, and G. Dolzmann, J. Mech. Phys. Solids **50**, 1431 (2002).
[15] J. M. Adams, S. Conti, and A. DeSimone, Cont. Mech. and Thermo. **18**, 319 (2007).
[16] P. D. Olmsted, J. Phys. II France **4**, 2215 (1994).
[17] R. Stannarius, V. Aksenov, J. Bläsing, A. Krost, M. Rössler, and R. Zentel, Phys. Chem. Chem. Phys. **8**, 2293 (2006).
[18] H. Finkelmann, I. Kundler, E. M. Terentjev, and M. Warner, J. de Phys. II **7**, 1059 (1997).
[19] W. Lehmann, H. Skupin, C. Tolksdorf, E. Gebhard, R. Zentel, P. Krüger, M. Lösche, and F. Kremer, Nature **410**, 447 (2001).
[20] E. Zubarev, S. Kuptsov, T. Yuranova, R. Talroze, and H. Finkelmann, Liq. Cryst. **26**, 1531 (1999).